Energy Proceedings
Vol 41, 2024
ISSN 2004-2965

Roadmap to Offshore Power-Liquid Hydrogen Co-production and Hybrid Delivery System Based on Superconducting Technology

Jian Yang[1], Yanzhong Li[1], Hongbo Tan[1*]

1 Institute of Refrigeration and Cryogenic Engineering, Xi'an Jiaotong University, Xi'an, 710049, PR China

([*] Corresponding Author: hongbotan@mail.xjtu.edu.cn)

ABSTRACT

As offshore wind farms (OWFs) evolve to larger scale and longer distance, superconducting technology has an opportunity for application. Liquid hydrogen (LH_2) is an ideal cooling medium for superconductors used in OWFs and is a high-quality product. Therefore, an offshore power-LH_2 co-production and hybrid delivery system based on superconducting technology is designed. The SEC, EXE, and COP of hydrogen liquefaction and subcooling integration process are 8.82 kWh/kg_{LH2}, 40.6%, and 0.15, respectively. LH_2 is produced to cool superconducting generators and transported ashore along with electricity using the hybrid energy pipeline. At a LH_2 delivery rate of 1 kg/s, the maximum delivery distance of the hybrid energy pipeline can reach 81.7 km.

Keywords: offshore wind power, liquid hydrogen production, superconducting generator, hybrid energy pipeline

1. INTRODUCTION

Offshore wind farms (OWF) are becoming more and more popular due to the small installation space constraints and high average wind speeds [1]. However, there are two problems associated with the development of large-scale OWFs. Firstly, due to the deep-water level and harsh environment, the installation of wind turbines in distant sea faces many technical difficulties [2]. Secondly, offshore wind is not easy to predict and has poor stability [3]. Superconducting technology and hydrogen production from offshore wind power are breakthroughs in solving these two problems.

Nam et al. [4] designed two superconducting generators using YBCO and MgB_2 wires respectively. Although the YBCO-based generator was smaller and lighter than the MgB_2-based generator, MgB_2 was more practical because it was easier to be manufactured into long wires and was cheaper. Electricity from OWFs can be used to electrolyze water to produce hydrogen, thereby smoothing the power characteristics of wind power [5-6]. A hybrid energy pipeline consisting of a cryogenic LH_2 pipeline and superconducting cables can accomplish efficient transmission of both chemical and electrical power [7-10].

As OWFs evolve to larger scale and longer distance, superconducting technology has an opportunity for application. In this study, an offshore power-LH_2 co-production and hybrid delivery system based on superconducting technology is developed.

2. OPTIMIZED DESIGN AND PERFORMANCE EVALUATION OF THE PROPOSED SYSTEM

An offshore power-LH_2 co-production and hybrid delivery system based on superconducting technology is displayed in Fig. 1. It mainly consists of an offshore superconducting wind power generation system, an offshore LH_2 production system, and a hybrid energy delivery pipeline.

Table 1 Energy consumption for LH_2 production.

Processes	Energy consumption
Seawater desalination [11]	0.03 kWh/kg_{LH2}
Electrolytic hydrogen production [12]	52.9 kWh/kg_{LH2}
Hydrogen liquefaction [13]	6.4 kWh/kg_{LH2}
LH_2 subcooling and pressurization	1.4 kWh/kg_{LH2}
Total	60.76 kWh/kg_{LH2}

The total installed capacity of the proposed system is 1 GW, and the design LH_2 production rate is 1 kg/s. The main energy-consuming processes involved in LH_2 production process include the desalination, electrolytic hydrogen production, hydrogen liquefaction and LH_2 subcooling processes. As listed in Table 1, the total energy consumption for LH_2 production is calculated to

This is a paper for 15th International Conference on Applied Energy (ICAE2023), Dec. 3-7, 2023, Doha, Qatar.

be 60.76 kWh/kg_{LH2} using typical energy consumption values for each process given in the literature. It can be calculated that the power required for LH_2 production of 1 kg/s is 218.74 MW, which is approximately 22% of the total power generation.

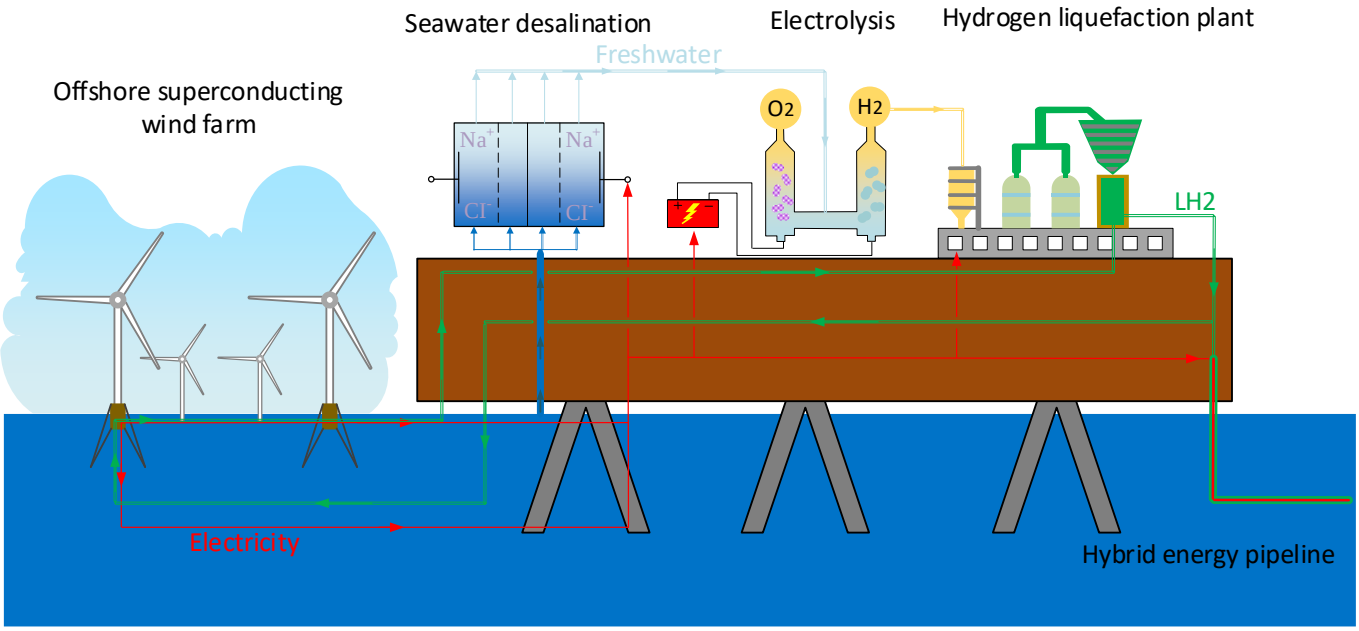

Fig. 1. Schematic diagram of the offshore power-LH_2 co-production and hybrid delivery system.

2.1 Offshore liquid hydrogen production system

The offshore LH_2 production system mainly includes a seawater desalination unit, a water electrolysis unit, and a hydrogen liquefaction unit. Among them, seawater reverse osmosis [11] and proton exchange membrane electrolysis [12] technologies are currently well-developed and can be applied at sea. A lot of improvement efforts have been made for hydrogen liquefaction processes to reduce the energy consumption [13,14]. However, no research has been reported for offshore hydrogen liquefaction systems. Therefore, an integrated process for offshore hydrogen liquefaction and subcooling is developed.

From previous study [14], the use of the Claude cycle for hydrogen liquefaction involves lower energy and investment costs and occupies less space than the helium Brayton refrigeration cycle. Therefore, an integrated hydrogen liquefaction and subcooling process is developed based on the Claude cycle, as shown in Fig. 2. A simple absorption refrigeration system with ammonia as the working fluid is used to pre-cool hydrogen to −30°C. An enhanced dual-stage Claude cycle is used for hydrogen liquefaction. Among them, the first refrigeration loop enables the cooling of hydrogen to −151°C. The second loop can cool hydrogen from −151°C to −235°C, exceeding the range of cooling that can be accomplished by a regular Claude cycle at the same pressure ratio. The helium Brayton cycle is used for the subcooling of LH_2.

2.1.1 Refrigeration process analysis

During the hydrogen liquefaction and subcooling process, refrigeration cycles are innovatively designed so that they can provide the cold energy required for hydrogen cooling at the corresponding temperature. An enhanced dual-stage Claude cycle is designed to provide cooling for hydrogen over a wider temperature range. The two refrigeration loops in the enhanced Claude cycle are not next to each other as those in a regular dual-stage Claude cycle, but are spaced by a heat exchanger (HX-3). This enables the hydrogen in the second loop to enter the expander at a lower temperature (−202°C), thereby significantly reducing the refrigeration temperature (−239.1°C). However, due to the lower mass flow rate, the return hydrogen cannot provide enough cold energy in HX-3. To solve this problem, the hydrogen in the second refrigeration loop is split into two streams. A portion of hydrogen (H22) is cooled to −239.1°C after full expansion, while another portion of hydrogen (H17) is only cooled to −224.3°C due to retaining a certain amount of pressure. This enables the latter portion of hydrogen to be used twice in HX-3 as refrigerants to cool

hydrogen, thus matching the heat flow to the cold flow in HX-3.

The enhanced dual-stage Claude cycle reduces the refrigeration temperature but results in insufficient cold energy in HX-5 due to the low mass flow rate of the low-temperature refrigerant stream (H22). Therefore, the required cold energy in HX-5 needs to be supplemented by the helium Brayton refrigeration cycle. The helium in the Brayton refrigeration cycle is also split into two streams. The temperature of a portion of helium (15) drops to −259.1°C after full expansion, while the temperature of another portion of helium (11) drops to −250.3°C after expansion because it retaining a certain amount of pressure. The latter can be used in HX-5 to supplement the cold energy as it can be re-cooled by expansion. As shown in Fig. 3, this portion of helium (10) is used as refrigerant in HX-5 and HX-6 until its temperature rises to −227°C (12). Then, it is mixed with another helium stream after lowering its temperature by further expansion.

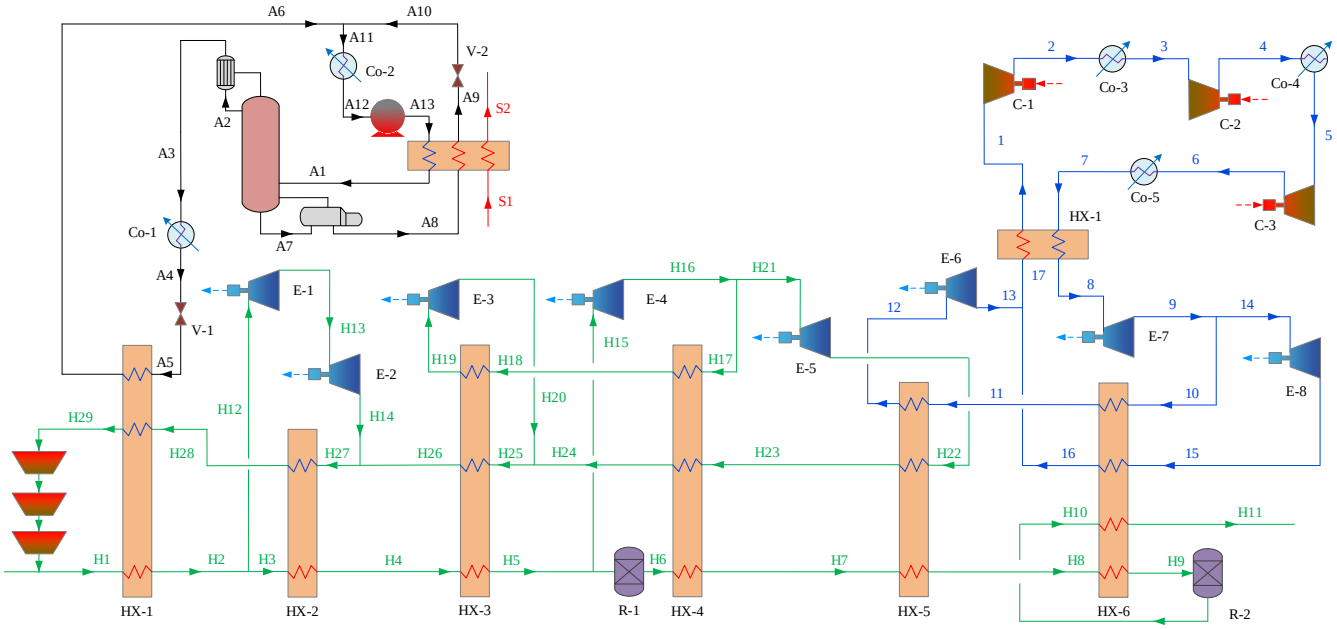

Fig. 2. Flowchart of the integrated hydrogen liquefaction and subcooling process.

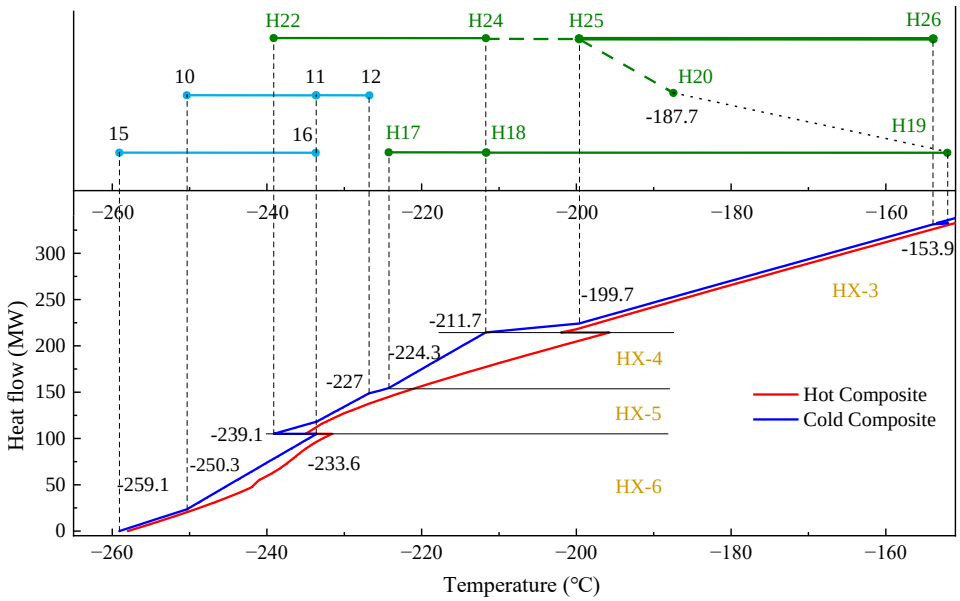

Fig. 3. Composite curves between hydrogen and refrigerants and the operating temperatures of refrigerant streams.

2.1.2 System thermodynamic analysis

The energy exchange between the integrated system and the external environment includes the energy output from expanders, and energy input from compressors and centrifugal pumps [15]. Assuming that the former is recovered and powered for hydrogen liquefaction, the net power of the integrated process can be calculated by Eq. (1).

$$\dot{W}_{\text{net}} = \dot{W}_{\text{P}} + \dot{W}_{\text{C}} - \dot{W}_{\text{E}} \tag{1}$$

To facilitate energy consumption comparison between hydrogen liquefaction systems with different capacities, specific energy consumption (SEC) is typically adopted as an energy indicator. It can be expressed by Eq. (2).

$$\text{SEC} = \frac{\sum \dot{W}_{\text{net}}}{\dot{m}_{\text{LH}_2}} \tag{2}$$

The exergy efficiency (EXE) and coefficient of performance (COP) are applied to measure the efficiency of exergy gain of hydrogen and heat removal from hydrogen [15], expressed by Eqs. (3) and (4).

$$\text{EXE} = \frac{\dot{m}_{\text{LH2}} \cdot \left(e_2 - e_1\right)}{\dot{W}_{\text{net}}} \tag{3}$$

$$\text{COP} = \frac{\dot{m}_{\text{LH2}} \cdot \left(h_1 - h_2\right)}{\dot{W}_{\text{net}}} \tag{4}$$

The thermodynamic performance indicators of the integrated system are listed in Table 2. The SEC, EXE and COP of the integrated system are 8.82 kWh/kg_{LH2}, 40.6% and 0.15, respectively. The energy consumption of the system is concentrated in the enhanced Claude cycle and helium Brayton refrigeration cycle. Since the heat source of the absorption refrigeration cycle is solar energy, its energy consumption is negligibly low. The lower the temperature, the more difficult it is to remove heat from hydrogen. Therefore, the COP of the Brayton refrigeration cycle for LH_2 subcooling is very low. However, the Brayton refrigeration cycle exhibits a high exergy efficiency since only a small amount of heat transfer is required to obtain high quality cold energy from refrigerant.

Table 2 Thermodynamic performance indicators of the integrated system.

Sections	SEC (kWh/kg_{LH2})	EXE (%)	COP
Absorption refrigeration cycle	0.005	-	-
Enhanced Claude cycle	4.00	38.8	0.22
Helium Brayton refrigeration cycle	4.82	45.0	0.05
Integrated process	8.82	40.6	0.15

2.2 Hybrid energy delivery pipeline

The cross-sectional structure of the hybrid energy pipeline used in this study is shown in Fig 4. The middle part of the pipe is the superconducting cable, which

consists of copper, MgB_2 cable, electrical insulation and shielding layer from inside to outside. On the outside of the superconducting cable is the ring-shaped channel, which is used to transport LH_2 and provide the required cryogenic condition for the superconducting cable. A cryostat insulated with multi-layers insulation is installed directly on the outside of the ring-shaped channel. Table 3 lists the structural parameters of the hybrid energy pipeline.

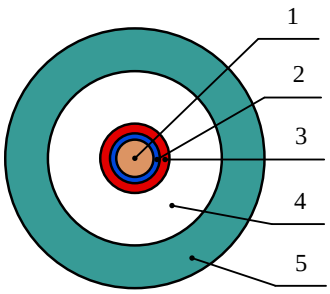

Fig. 4. The cross-sectional structure

Table 3 Structural parameters of the hybrid energy pipeline.

Number	Name	Outside diameter (mm)
1	Copper	30
2	MgB_2 cable	34.5
3	Insulation and shielding layer	47.5
4	LH_2 main channel	120
5	Cryostat	183

Table 4 The parameters required for the thermal-hydraulic calculation.

Terminal *p*	Terminal *t*	Heat input	Roughness	Fluid	Thermodynamic parameters	Friction factor
400 kPa	25 K	1 W/m	0.06 mm	para-H_2	REFPROP	Colebrook-White

2.2.1 Simplification of one-dimensional compressible flow equations

Thermal-hydraulic calculation for LH_2 cryogenic piping is performed by being simplified to a one-dimensional compressible flow form. Neglecting the change in potential energy, a simplified form of one-dimensional compressible flow equations that consider the fluid compressibility through the introduction of thermal expansivity factor is derived as shown below [10].

$$\frac{1}{\rho}\frac{\mathrm{d}p}{\mathrm{d}x} = -\left(1+\frac{\alpha_v u^2}{C_p}\right)F - \frac{\alpha_v u^2}{C_p}\frac{q}{m} \tag{5}$$

$$C_p\frac{\mathrm{d}T}{\mathrm{d}x} = (1-\alpha_v T)F + \frac{q}{m} \tag{6}$$

where p and T are LH_2 pressure and temperature, m and u are LH_2 mass flow rate and velocity, α_v is thermal expansivity factor of LH_2, q is the total thermal income towards LH_2, and F is related to the friction factor. The parameters required to perform the thermal-hydraulic calculation for the hybrid energy pipeline are listed in Table 4.

2.2.2 Delivery performance evaluation of the pipeline

The maximum delivery distance of the hybrid energy pipeline can be calculated with the solidification parameters of LH_2 as initial boundary conditions. Fig.5 illustrates the temperature rise and pressure drop profiles along the pipeline. At a diameter of 0.12 m of the ring-shaped channel and a LH_2 delivery rate of 1 kg/s, the maximum delivery distance of the hybrid energy pipeline can reach 81.7 km. The initial pressure of LH_2 entering the pipeline is 2084 kPa, which corresponds to a solidification temperature of 14.5 K. It follows that by providing subcooling and pressurization to LH_2, the hybrid energy pipeline satisfies most current OWFs in terms of delivery distance.

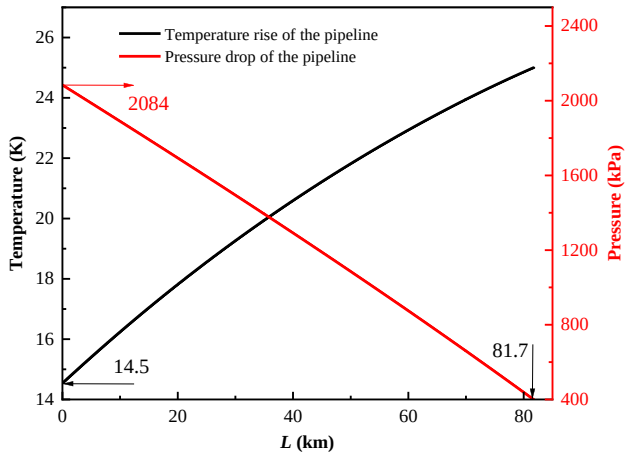

Fig. 5. Temperature rise and pressure drop profiles along the hybrid energy pipeline.

The effect of the mass flow rate of LH_2 and the diameter of the ring-shaped channel on the delivery performance of the hybrid energy pipeline is investigated. The delivery capacity of the hybrid energy pipeline with different ring-shaped channel diameters at a LH_2 mass flow rate of 1 kg/s is shown in Fig. 6(a). The curves in Fig. 6 show the initial pressures and temperatures of LH_2 required for the pipeline with different delivery distances. As the diameter increases, the maximum delivery distance of the hybrid energy

pipeline can be increased from 50 km to more than 90 km. It follows that an increase in the diameter is most beneficial in enhancing the delivery capacity of hybrid energy pipelines, but requires more capital investment.

As shown in Fig. 6(b), the delivery capacity of the hybrid energy pipeline with a ring-shaped channel diameter of 0.12 m is calculated for different LH_2 mass flow rates. On the one hand, an increase in LH_2 mass flow rate will significantly increase the viscous losses, thereby discouraging the delivery of LH_2. On the other hand, it can slow down the temperature rise of LH_2 along the line, which contributes to the extension of the delivery distance. Therefore, he delivery capacity of pipeline exhibits less sensitivity to changes in the mass flow rate of LH_2. Thanks to this delivery property, the amount of LH_2 produced can be varied within a certain range to cope with power fluctuations in the OWF and the curtailment of the power grid.

3. CONCLUSIONS

In this study, an offshore power-LH_2 co-production and hybrid delivery system based on superconducting technology is developed and evaluated. The main efforts and conclusions drawn are as follows:

1. Bulky regular generators are replaced with highly efficient superconducting generators and LH_2 is utilized to cool superconducting generators. Submarine collector cables may have the same topology as submarine LH_2 pipelines and be laid in the same trench.

2. An integrated offshore hydrogen liquefaction and subcooling process based on an enhanced Claude cycle is proposed. The SEC, EXE, and COP of the integrated process are 8.82 kWh/kg_{LH2}, 40.6%, and 0.15.

3. At a diameter of 0.12 m of the ring-shaped channel and a LH_2 delivery rate of 1 kg/s, the maximum delivery distance of the hybrid energy pipeline can reach 81.7 km. An increase in the diameter of ring-shaped channel can significantly increase the delivery distance.

DECLARATION OF INTEREST STATEMENT

The authors declare that they have no known competing financial interests or personal relationships that could have appeared to influence the work reported in this paper. All authors read and approved the final manuscript.

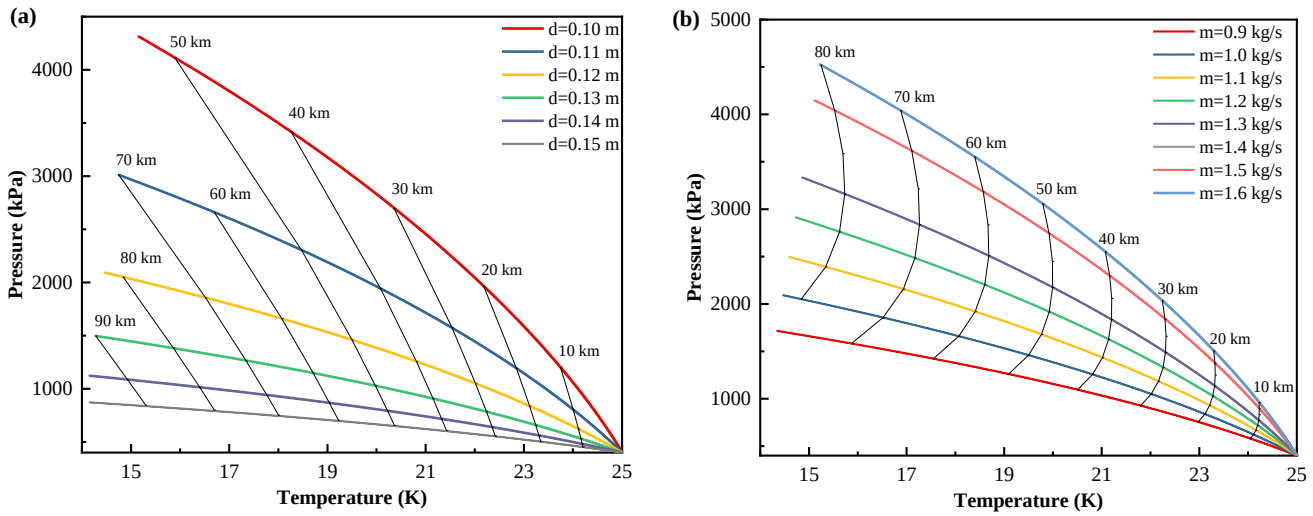

Fig. 6. Analysis of parameters affecting the delivery performance of the hybrid energy pipeline: (a) diameter of ring-shaped channel, (b) mass flow rate of LH_2.

REFERENCE

[1] Perveen R, Kishor N, Mohanty SR. Off-shore wind farm development: Present status and challenges. Renew Sust Energy Rev 2014;29:780-792.

[2] Díaz H, Soares CG. Review of the current status, technology and future trends of offshore wind farms. Ocean Eng 2020;209:107381.

[3] Bonacina CN, Gaskare NB, Valenti G. Assessment of offshore liquid hydrogen production from wind power for ship refueling. Int J Hydrogen Energy 2022;47:1279-1291.

[4] Nam GD, Sung HJ, Go BS, Park MW, Yu IK. Design and comparative analysis of MgB2 and YBCO wire-based-superconducting wind power generators. IEEE T Appl Supercon 2018;28:5205605.

[5] Apostolou D, Enevoldsen P. The past, present and potential of hydrogen as a multifunctional storage application for wind power. Renew Sust Energy Rev 2019;112:917-929.
[6] Babarit A, Gilloteaux JC, Clodic G, Duchet M, Simoneau A, Platzer MF. Techno-economic feasibility of fleets of far offshore hydrogen-producing wind energy converters. Int J Hydrogen Energy 2018;43:7266-7289.
[7] Grant PM. The supercable: Dual delivery of chemical and electric power. IEEE T Appl Supercon 2005;15:1810-1813.
[8] Trevisani L, Fabbri M, Negrini F. Long distance renewable-energy-sources power transmission using hydrogen-cooled MgB2 superconducting line. Cryogenics 2007;47:113-120.
[9] Yamada S, Hishinuma Y, Uede T, Schippl K, Motojima O. Study on 1 GW class hybrid energy transfer line of hydrogen and electricity. J Phys Conf Ser 2008;97:012167.
[10] Vysotsky VS, Antyukhov IV, Firsov VP, et al. Energy transfer with hydrogen and superconductivity – the review of the first experimental results. Physics Procedia 2015;65:299-302.
[11] Lin SS, Zhao HY, Zhu LP, et al. Seawater desalination technology and engineering in China: A review. Desalination 2021;498:114728.
[12] d'Amore-Domenech R, Leo TJ. Sustainable hydrogen production from offshore marine renewable farms: Techno-energetic insight on seawater electrolysis technologies. ACS Sustain Chem Eng 2019;7:8006-8022.
[13] Yang J, Li YZ, Tan HB, Bian J, Cao XW. Optimization and analysis of a hydrogen liquefaction process integrated with the liquefied natural gas gasification and organic Rankine cycle. J Energy Storage 2023;59:106490.
[14] Yang J, Li YZ, Tan HB. Integrated hydrogen liquefaction process with a dual-pressure organic Rankine cycle-assisted LNG regasification system: Design, comparison, and analysis. Appl Energy 2023;347:121372.
[15] Yang J, Li YZ, Tan HB. Study on performance comparison of two hydrogen liquefaction processes based on the Claude cycle and the Brayton refrigeration cycle. Processes 2023;11:932.